Land contribution to natural CO_2 variability on time scales of centuries

Rainer Schneck,[1] Christian H. Reick,[1] and Thomas Raddatz[1]

Received 1 November 2012; revised 16 March 2013; accepted 4 April 2013; published 10 June 2013.

[1] The present paper addresses the origin of natural variability arising internally from the climate system of the global carbon cycle at centennial time scales. The investigation is based on the Max Planck Institute for Meteorology, Coupled Model Intercomparison Project Phase 5 (MPI-MCMIP5) preindustrial control simulations with the MPI Earth System Model in low resolution (MPI-ESM-LR) supplemented by additional simulations conducted for further analysis. The simulations show a distinct low-frequency component in the global terrestrial carbon content that induces atmospheric CO_2 variations on centennial time scales of up to 3 ppm. The main drivers for these variations are low-frequency fluctuations in net primary production (NPP) of the land biosphere. The signal arises from small regions scattered across the whole globe with a pronounced source in North America. The main reason for the global NPP fluctuations is found in climatic changes leading to long-term variations in leaf area index, which largely determines the strength of photosynthetic carbon assimilation. The underlying climatic changes encompass several spatial diverse climatic alterations. For the particular case of North America, the carbon storage changes are (besides NPP) also dependent on soil respiration. This second mechanism is strongly connected to low-frequency variations in incoming shortwave radiation at the surface.

Citation: Schneck, R., C. H. Reick, and T. Raddatz (2013), Land contribution to natural CO_2 variability on time scales of centuries, *J. Adv. Model. Earth Syst.*, *5*, 354–365, doi:10.1002/jame.20029.

1. Introduction

[2] Global atmospheric CO_2 concentrations vary on time scales ranging from millions of years to hours, but the understanding of the processes leading to these variations is usually rather qualitative. It is clear that the causes must be different at the different time scales [*Doney and Schimel*, 2007]. For example, long-term CO_2 changes in the course of the last 60 Ma are attributed mainly to geological processes like volcanic, hydrothermal, and metamorphic outgassing and weathering of silicate minerals or limestone formation [*Pearson and Palmer*, 2000; *Zachos et al.*, 2008]. It is generally accepted that time scales of ~400 to ~20 kyr orbital cycles can affect the atmospheric CO_2 concentration by triggering glacial ages, although the details of these processes are far from being fully understood [*Zachos et al.*, 2001; *Petit et al.*, 1999; *Sigman and Boyle*, 2000; *Brovkin et al.*, 2007; *Siegenthaler et al.*, 2005a; *Caillon et al.*, 2003]. There are indications that glacials and interglacials are associated with sequences of events leading to CO_2 changes also at shorter time intervals, but the exact mechanisms are unclear [see *Prentice et al.*, 2001; *Ruddiman et al.*, 2011]. Particularly uncertain is a possible relation between solar activity and atmospheric CO_2: indications found by *Keeling and Whorf* [1995] that solar cycles may induce decadal oscillations of atmospheric CO_2 are mostly correlational. In contrast, it is comparably well understood that on yearly time scales volcanic eruptions can alter atmospheric CO_2 [*Robock*, 2003; *Brovkin et al.*, 2010]. Almost periodic atmospheric CO_2 variations may arise from El Nino Southern Oscillation, an internal climate mode with a period around 4–5 years [*Bacastow*, 1976; *Bacastow et al.*, 1980; *Raddatz et al.*, 2007; *Schwalm et al.*, 2011], but the exact connections are still under discussion [*Rayner and Law*, 1999; *Bosquet et al.*, 2000]. Finally, at subannual time scale variations of atmospheric CO_2 are largely understood: the seasonal variation arises from the asymmetric north–south distribution of continents so that the seasonality of northern hemisphere photosynthesis dominates the atmospheric CO_2 signal [*Keeling et al.*, 1993], and the daily cycle of atmospheric CO_2 arises from the day/night contrast of plant CO_2 uptake.

[3] For centennial time scales, the knowledge about CO_2 variability is mainly based on ice core data for the last 2 kyr with a temporal resolution not below a decade [e.g., *MacFarling Meure et al.*, 2006; *Siegenthaler et al.*, 2005a, 2005b; *Etheridge et al.*, 1996; *Ahn et al.*, 2012]. CO_2 reconstructions reaching back beyond the Holocene do not capture variability of time scales below centuries [cf. *Lüthi et al.*, 2008]. Several mechanisms could have caused these CO_2 variations. Based on δ^{13} CO_2

[1]Max Planck Institute for Meteorology, Hamburg, Germany.

1942-2466/13/jame.20029

data from Law Dome ice cores the CO_2 reduction during the Little Ice Age (LIA, ~1500–1750 A.D.) is explained by *Joos et al.* [1999] and *Trudinger et al.* [2002] as a result of land C uptake and oceanic outgassing. By using a simple box carbon model for the LIA, *Trudinger et al.* [1999, 2005] demonstrate that a prescribed temperature reduction increases C uptake by the land biosphere and leads to similar atmospheric CO_2 variations as reconstructed from ice cores. This "temperature" explanation is also supported by *Etheridge et al.* [1996] who argue that the LIA CO_2 decrease is caused by the cooling and not vice versa. The studies of *Jungclaus et al.* [2010], *Brovkin et al.* [2010], and *Gerber et al.* [2003] also fit to this explanation. They simulated the effects of solar and volcanic activities on climate and the carbon cycle for the last millennium. Both forcings together may have cooled the climate for hundreds of years after the medieval optimum, which could then explain changes in atmospheric CO_2. However, the size of the effects is rather uncertain as has explicitly been demonstrated by *Jungclaus et al.* [2010]. During the last 300 years, CO_2 variability on centennial time scales is considerably influenced by anthropogenic land cover changes (ALCCs) and emissions from fossil fuel burning [*Forster et al.*, 2007; *Pongratz et al.*, 2009; *Pongratz et al.*, 2010; *Reick et al.*, 2010]. Anthropogenic influence due to vegetation cover changes may have already started near the Pleistocene-Holocene boundary [*Pinter et al.*, 2011; *Williams*, 2003], but the contribution to atmospheric CO_2 alterations is lively debated and cannot be exactly quantified yet [see *Stocker et al.*, 2011; *Pongratz et al.*, 2009].

[4] It is quite plausible that even without external forcing the internal climate variability might lead to variations in atmospheric CO_2. In a 1000 year Earth System Model (ESM) simulation by *Doney et al.* [2006] at constant preindustrial conditions, the yearly averages of atmospheric CO_2 vary about 4 ppm on time scales of centuries. Their results indicate that atmospheric CO_2 is dominated by variations of the terrestrial C storage due to regional changes in net primary production (NPP). The oceanic contribution to CO_2 variability turned out to be much weaker and led to a dampening of the land-induced atmospheric CO_2 variability. *Doney et al.* [2006] use the NCAR CSM 1.4 model (National Center for Atmospheric Research Climate Systems Model) consisting of the physical components for ocean, atmosphere, land, and sea ice, coupled to carbon models for land and ocean. As compared to our experiments presented here, their simulations are conducted with a somewhat weaker atmospheric and land resolution of T31 with 18 vertical atmosphere levels and an ocean sea ice resolution of 0.8°–1.8° latitude and 3.6° longitude with 25 oceanic levels. Their model does not include an explicit nitrogen cycle, fires and other disturbances, herbivory, dynamic vegetation cover, or ALCC. Another hint for intrinsic atmospheric CO_2 variability is found in a similar simulation for preindustrial conditions by *Jungclaus et al.* [2010]. In their study the 5th–95th percentile of a 31 year running mean of atmospheric CO_2 spans about 2 ppm.

[5] In the present paper, we examine the contribution of internal climate variability to centennial variations of atmospheric CO_2. Our special focus will be on the land contribution to the C storage changes because it turns out that the centennial variability we see in our simulations is dominated by the land carbon dynamics. This study is based on the preindustrial control simulations performed with the MPI ESM (MPI-ESM-LR) that were done as part of CMIP5 community simulations [*Taylor et al.*, 2011a], supplemented by some additional simulations performed with the same model to address particular questions. In section 2 we describe the MPI-ESM land component JSBACH. For a detailed description of the other components of the MPI-ESM, we refer the reader to the articles of B. Stevens et al. (The atmospheric component of the MPI Earth System Model: ECHAM6, submitted to *Journal of Advances in Modeling Earth Systems*, 2012, hereinafter referred to as Stevens et al., submitted manuscript, 2012), J. H. Jungclaus et al. (Characteristics of the ocean simulations in MPIOM, the ocean component of MPI-Earth System Model, submitted to *Journal of Advances in Modeling Earth Systems*, 2012), C. H. Reick et al. (The representation of natural and anthropogenic landcover change in MPI-ESM, submitted to *Journal of Advances in Modeling Earth Systems*, 2012, hereinafter referred to as Reick et al., submitted manuscript, 2012), and T. Ilyina et al. (The global ocean biogeochemistry model HAMOCC: Model architecture and performance as component of the MPI-Earth System Model in different CMIP5 experimental realizations, submitted to *Journal of Advances in Modeling Earth Systems*, 2012). In section 3 we describe the experimental design, and section 4 presents the results. Section 5 closes with the discussion and conclusions.

2. Land Physics and Biosphere Model JSBACH

[6] JSBACH is the land component of MPI-ESM. Technically, it is part of the atmosphere model ECHAM6 (European Center HAMburg, see Stevens et al., submitted manuscript, 2012) and runs on the same grid. JSBACH inherits the physics components (surface radiation and energy balance, soil hydrology, soil heat transport) from ECHAM5 [*Roeckner et al.*, 2003]. Vegetation is represented by eight PFTs (plant functional types) for natural vegetation, namely, tropical and extratropical deciduous and evergreen trees, two types of shrubs (deciduous and raingreen), as well as C3 and C4 grasses. Agricultural vegetation is represented by a C3 crop PFT, and two pasture PFTs (C3, C4). The leaf area index (LAI) of all PFTs is computed fully dynamically in interaction with climate. The distribution of vegetation and deserts changes in interaction with climate [*Brovkin et al.*, 2009; Reick et al., submitted manuscript, 2012] and determines in combination with the LAI and snow cover the land surface albedo [*Otto et al.*, 2011].

[7] Of particular interest for the present study is the land carbon cycle in JSBACH. The biogeochemical components (canopy radiation, photosynthesis, autotrophic respiration) are partly taken over from the BETHY model [Biosphere-Energy-Transfer-Hydrology Model, *Knorr*, 2000]. Every model time step, from PAR (photosynthetically active part of net shortwave radiation) and

depending on the LAI first fAPAR (fraction of PAR absorbed in the vegetation canopy), is computed for each PFT. Entering this into the appropriate photosynthesis scheme (C3 after *Farquhar et al*. [1980] and C4 after *Collatz et al*. [1992]), and accounting for temperature and soil water availability, gross primary productivity (GPP) is determined. By scaling the leaf respiration as obtained from photosynthesis to the whole plant autotrophic respiration R_a, net primary productivity is obtained from NPP = GPP − R_a. Using a simple allometry [*Wolf et al*., 2011], NPP is distributed to three vegetation carbon pools (living tissues, carbohydrate and starch storage, and wood). Depending on the phenological changes of the LAI, and depending on plant aging, carbon is transferred to the four aboveground and belowground pools for litter from the woody and nonwoody parts (e.g., leaves) of vegetation. In addition, there is a transfer of carbon to the litter pools and the atmosphere by wildfires, herbivory (grazing), and harvest of agricultural lands. However, the contribution of these transfers to the carbon variability addressed in this paper is negligible for all of the presented simulations. The temperature dependence of litter decomposition is described by a Q10 formula [*Lloyd and Taylor*, 1994], combined with a linear dependence on relative soil moisture content [*Knorr*, 2000]. The turnover times for woody and nonwoody litter decomposition are about (dependent on the PFT) 30 and 2 years, respectively. Upon litter decomposition, part of the respired carbon is given back to the atmosphere, whereas the remaining more recalcitrant components of organic carbon are put into a pool for soil carbon, which is also decomposed according to the same Q10 model as the litter carbon, but with a turnover time of approximately 100 years. The total carbon flux from the litter pools and the soil pool is called heterotrophic respiration (R_h).

[8] One peculiarity of JSBACH is that the whole submodel for land cover change and land carbon can be run independently from the rest of JSBACH. It is forced by JSBACH data (e.g., from a fully coupled MPI-ESM run) and can reproduce land cover and carbon to numerical accuracy. The carbon pools are normally restarted from the balanced state of a coupled MPI-ESM run, therefore its name *Cbalone*. Cbalone includes wind and fire damage as well as land use change and is driven by daily time series of NPP, LAI, soil temperature, relative soil moisture, and wind speed. The big advantage of Cbalone is that one can use the same JSBACH forcing for several runs but with different configurations (e.g., with and without natural vegetation dynamics or with different land use changes). This allows a direct comparison of the Cbalone output data for exactly the same forcing. However, by changing the configuration the model may get inconsistent with its forcing data since the land cover is decoupled from ECHAM and cannot feed back to climate.

3. Simulations

[9] An overview over the simulations is given in Table 1. The analysis of natural CO_2 variability is based on two slightly different simulations of preindustrial climate and carbon cycle with MPI-ESM-LR that have been conducted as part of the CMIP5 community simulations. The first of these simulations, denoted *CTL* control, is a fully coupled model run with external conditions representing the year 1850. The forcing is held constant during the integration. The orbital parameters for the year 1850 are taken from *Bretagnon and Francou* [1988], and solar irradiance is calculated as average over the years 1844–1856 derived from the SPARC/SOLARIS project http://sparcsolaris.geomar.de/cmip5.php). CO_2, CH_4, N_2O, CFC-11 (ChloroFluoroCarbon), and CFC-12 concentrations for the year 1850 are from the IIASA RCP database (International Institute for Applied Systems Analysis Representative Concentration Pathways, http://www.iiasa.ac.at/web-apps/tnt/RcpDb). For ozone, monthly concentrations are used (averaged over the years 1850–1860). Volcanic and anthropogenic aerosol forcing is not represented, and natural tropospheric aerosol forcing is based on the global aerosol data set from S. Kinne et al. (A new global aerosol climatology for climate studies, submitted to *Journal of Advances in Modeling Earth Systems*, 2012). In the LR version of MPI-ESM the resolution of ECHAM6 is set to T63 (i.e., about 2° horizontal resolution at the equator) with 47 vertical σ levels, and the ocean model MPIOM is driven at a resolution of GR15 (Grid Resolution 15, meaning a horizontal resolution of about 1.5°) and 40 z levels. For more information about the experimental design and the boundary conditions, see *Taylor et al*. [2011a] and M. Giorgetta et al., Climate change from 1 1850 to 2100 in MPI-ESM simulations for the Coupled Model Intercomparison Project 5, submitted to *Journal of Advance in Modeling Earth Systems*, submitted, 2013. under the

Table 1. Overview Over the Experiments

Experiment	Description
CTL	Experiment name in CMIP5 syntax: *esmControl_r1i1p1-LR* [see *Taylor et al*., 2011b, 2012]. One thousand year preindustrial run with all components of the MPI-ESM-LR fully coupled.
CTL_fixedCO2	Experiment name in CMIP5 syntax: *piControl_r1i1p1-LR* [*Giorgetta et al*., 2012]. As CTL but the atmospheric CO_2 concentration is prescribed with 285 ppm. We extended this run for further 450 years.
CTL_fixedCO2+Veg	As CTL_fixedCO2 but the vegetation cover remains fixed at the 1850 state.
CB_fixedCO2+Veg	Cbalone run for 1000 years with forcing from the 1000 years of CTL_fixedCO2. After 1000 years the forcing is repeated in the extension run.
CB_CTL	Cbalone run for 1150 years with repeated forcing of the same yearly cycle representing the average from 1000 years of CTL_fixedCO2.
CB_NPP	Cbalone run for 1000 years with the same yearly cycle as CB_CTL, except that the NPP forcing is taken from CTL_fixedCO2 and varies in time.

term piControl. The MPI-ESM-LR model calculates the carbon cycle dynamically in this experiment. Terrestrial C storage changes without CO_2 changes in the atmosphere are obtained from the so-called *CTL_fixedCO2* simulation, which is identical to CTL, except that the atmospheric CO_2 concentration is fixed to 285 ppm. We extended MPI-ESM-LR CMIP5 CTL_fixedCO2 run for further 450 years to see if there is a periodicity in the land carbon pools.

[10] To test how strong the land C storage changes of piControl_r1i1p1-LR depend on the vegetation dynamics, we repeated the CTL_fixedCO2 experiment with the vegetation cover fixed to the state of the year 1850. In the following this run is referred to as *CTL_fixedCO2+Veg*.

[11] To separate the C storage effects in CTL_fixedCO2 that are caused by changes in the vegetation cover from those that are caused by the atmospheric forcing, we performed an additional simulation with the Cbalone model (in the following referred to as *CB_fixedCO2+Veg*). The vegetation cover herein is fixed to the year 1850 state, and the forcing (see model description earlier) is taken from the 1000 years of CTL_fixedCO2. In this run the C storage of the land represents the storage that would appear with the 1850 vegetation under the forcing of CTL_fixedCO2. In contrast to the CTL_fixedCO2+Veg run, it still responds to the vegetation feedbacks on climate that are included in the atmospheric forcing of CTL_fixedCO2. We extended this run for further 1000 years and repeated the forcing to see how the carbon pools develop under the same 1000 year forcing but from another initial state. For our further analyses, we had to test in how far the NPP input to the Cbalone model can explain C storage variations in CB_fixedCO2+Veg. For that we had to run Cbalone with all input variables fixed. Due to the natural variations within these variables, we fixed them to an average state. First, we calculated for each input variable of Cbalone a single course of 1 year from the 1000 years of the CB_fixedCO2+Veg input. For that, each day in this year is calculated as a 1000 day average (from the corresponding day within the 1000 years). With this average forcing year, we run the so-called *CB_CTL* simulation for 1150 years until the terrestrial C pools reached equilibrium. From this equilibrium state we continued the simulation for further 1000 years with the constant forcing except of NPP. NPP in this run is taken from CB_fixedCO2+Veg and varies in time. The simulation is referred to as *CB_NPP* in the following.

4. Results

4.1. Carbon Storage Variations in the Fully Coupled Run

[12] In CTL the 21 year running mean of atmospheric C varies up to 6 PgC (or ~3 ppm) within 100 years

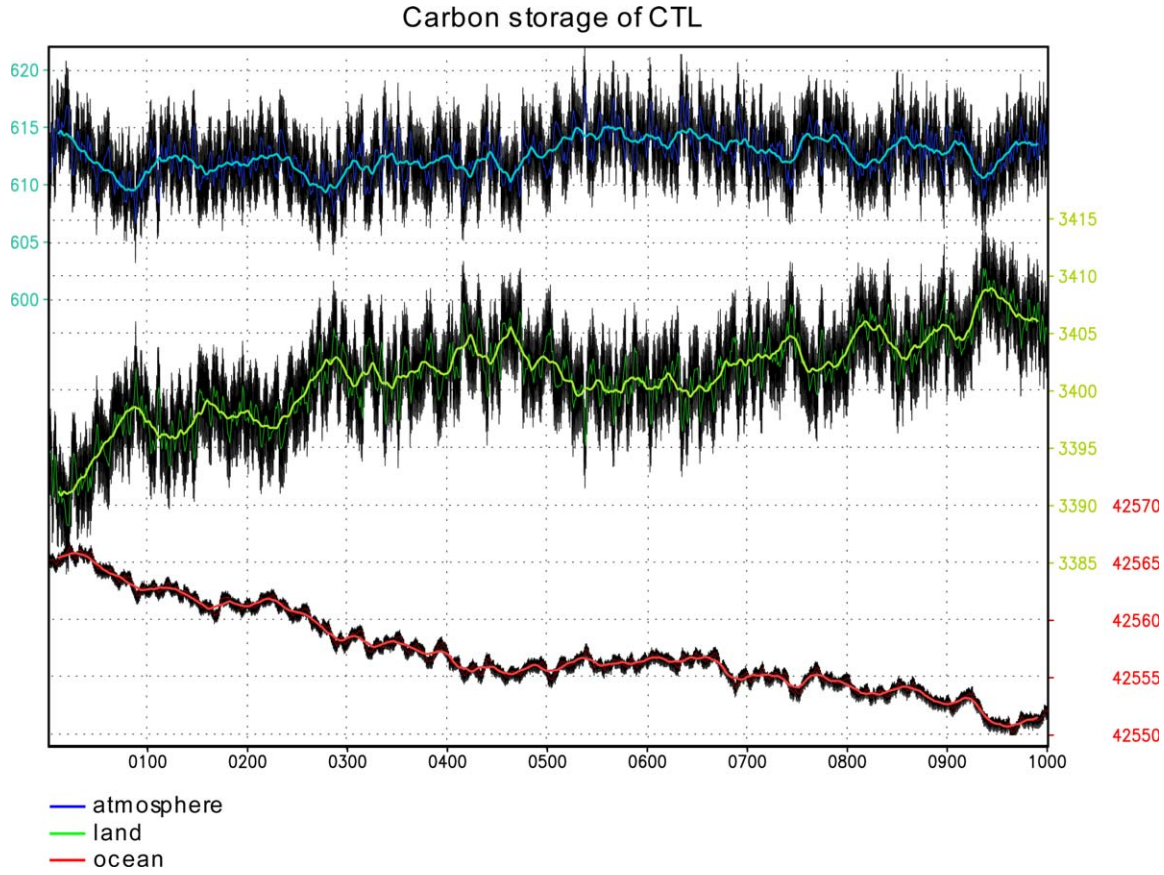

Figure 1. Carbon storage of CTL in atmosphere (blue), land (green), and ocean (red; PgC). Black lines represent

(Figure 1). Although atmospheric C shows no significant overall trend, land and ocean C storage has compensatory overall trends: for land C, this trend is positive and shows centennial variations somewhat stronger than seen in the atmosphere (up to 8 PgC). The overall increase on land is counterbalanced by a decrease of C storage in the ocean. This relative small model disequilibrium as compared to the absolute values should not affect the regarded variability in this paper. From the anticorrelation of the land C storage with both the atmospheric and the oceanic C content, it follows that the land component is the driving force for the centennial changes (C conservation). (Pearson's R^2 of the linear detrended 21 year running means between land and atmosphere is 0.21 and has the same value between land and ocean.) The ocean generally shows much weaker variations on time scales below 200 years than land or atmosphere.

4.2. Land Contribution to Carbon Storage Variability

[13] Since the atmospheric CO_2 concentration is fixed in CTL_fixedCO2, the land compartment develops its C pools without the influence of storage changes in the other Earth system compartments. In CTL, for example, increasing land C uptake by CO_2 fertilization decreases the atmospheric CO_2 concentration which then dampens the CO_2 fertilization. This dampening effect is blocked in CTL_fixedCO2. The long-term variability of terrestrial C doubles in CTL_fixedCO2 (Figure 2) as compared to CTL. At first sight, it seems that there is a ~250 year periodicity in the land C, but Figure 3b does not indicate strongly pronounced values in the power spectrum as compared to the random collections. This ~250 year periodicity is not seen in CTL (see Figures 1 and 3a). However, the variations on centennial time scales are strong in *CTL_fixedCO2*: up to ~15 GtC within 100 years for the 21 year running mean, which in the absence of compensatory CO_2 fluxes would correspond to ~4 ppm in the atmosphere when we assume that 1 ppm (CO_2) corresponds to 2.123 PgC [*Enting et al.*, 1994] and that land and ocean would compensate 40% of the changes [*Hansen and Sato*, 2004]. In the following sections, we analyze the reasons for the observed centennial variability in land carbon storage.

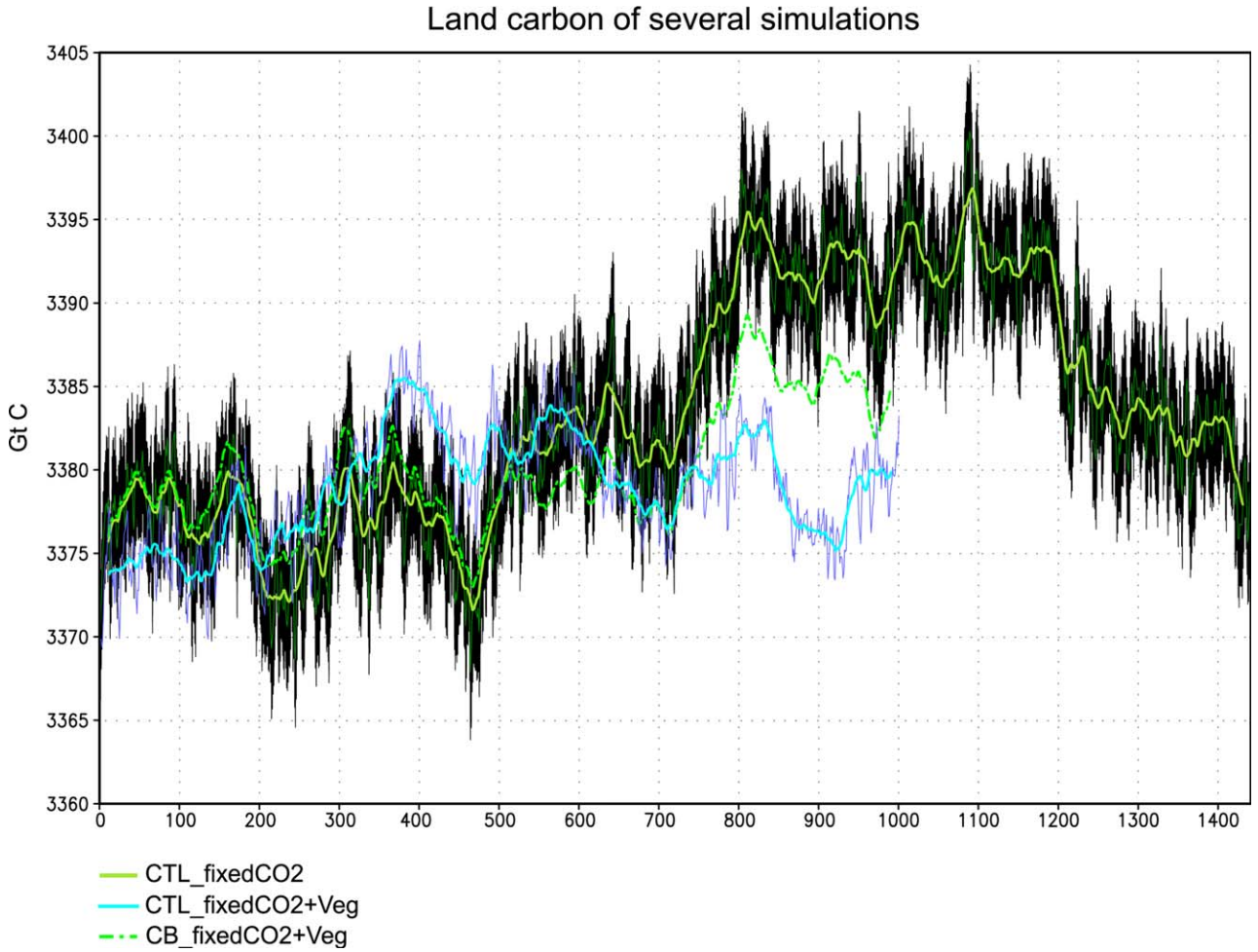

Figure 2. Carbon storage of CTL_fixedCO2 (light green), CB_fixedCO2+Veg (dark green, extension run not plotted), and CTL_fixedCO2+Veg (cyan; PgC). Black and dark green lines represent monthly and yearly means of

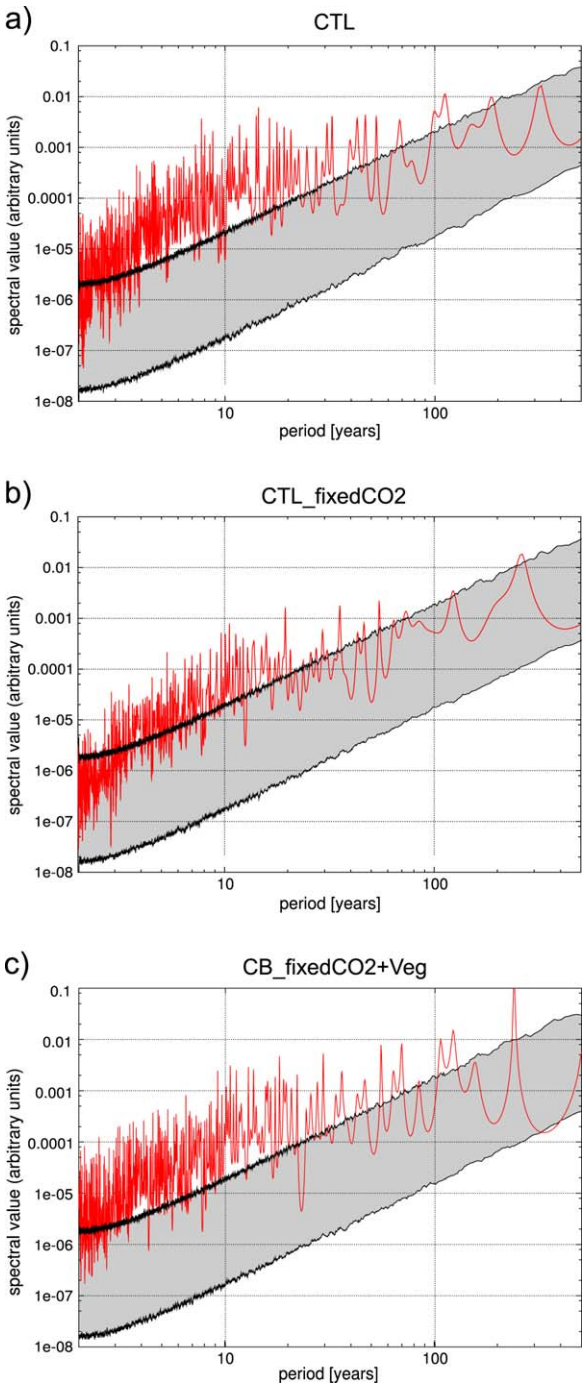

Figure 3. Spectrum of land carbon variability in (a) CTL, (b) CTL_fixedCO2, and (c) CB_fixedCO2+Veg. Spectrum computed by the All Poles method [*Press et al.*, 1992], after detrending with Legendre polynomials of order 3. All spectral values are divided by their integral over all periods. In red the simulation results, and in black the 5% and 95% quantiles of 2000 random Markov chain collections (from the corresponding simulation results after detrending). It should be noted that with longer periods the associated spectral value gets less representative for the model system since fewer cycles could be realized within the data.

4.3. Climatic Causes for the Centennial Land Carbon Variability

[14] The CTL_fixedCO2+Veg and CB_fixedCO2+Veg results (Figure 2) show that long-term terrestrial C variations also occur with similar strength as in CTL_fixedCO2 even when the vegetation dynamics is switched off. The power spectrum of CB_fixedCO2+Veg shows a similar peak as CTL_fixedCO2 at the ~250 year frequency (Figure 3c). From the positive land C trends of the first 1000 simulation years of CTL_fixedCO2, one could assume that the vegetation is not in equilibrium with climate. However, the negative trend of the extension of CTL_fixedCO2 indicates that this assumption is not correct. Furthermore, in the extension run of the CB_fixedCO2+Veg simulation, the initially different C pools of the extension run reach after only 100 simulation years nearly the same state again as before in CB_fixedCO2+Veg (not shown). Afterward, when the C pools of the extension run are again in equilibrium with climate, they follow the same line as in the first 1000 years of CB_fixedCO2+Veg. Accordingly, there is no long-term disequilibrium between vegetation and climate.

4.4. Geographical Origin of the Centennial Land C Variability

[15] In CTL_fixedCO2, a relatively small signal within the natural variability accumulates to centennial variations (Figure 2). Thus, a main task for the following analysis is to separate this signal from the noise. In the following, we analyze the CB_fixedCO2+Veg run since it includes most of the long-term C variability of CTL_fixedCO2 but excludes the effects of the vegetation dynamics (besides its implicit influence via the Cbalone forcing data that were generated from the CTL_fixedCO2 simulation that included the vegetation dynamics). To identify those areas which continuously contribute to the centennial land carbon variations, we built the 21 year running mean for each grid cell and detrended the time series. The same was done for the total land average shown in Figure 2. Then we calculated Pearson's correlation coefficient R^2 between the time series of the single grid cells and the total land average. The map of the correlation strength shows that regions all over the world contribute to the long-term changes of terrestrial C (Figure 4). At first view, it seems that these regions are distributed randomly over the globe (except for the cluster of positive correlations in North America). However, due to the relatively long time series the p values (probability to reach the same or a better correlation just by chance) on the contributing grid cells are very low, especially for grid cells with $R^2 \geq 0.1$ the p values remain below 10^{-5}. Furthermore, to test in addition also the stability of the pattern, we halved the time series used for the correlation calculation in Figure 4 and repeated the calculation for each part separately. As a result, the same pattern was found for both parts (not shown) so that the geographic pattern turns out to be stable.

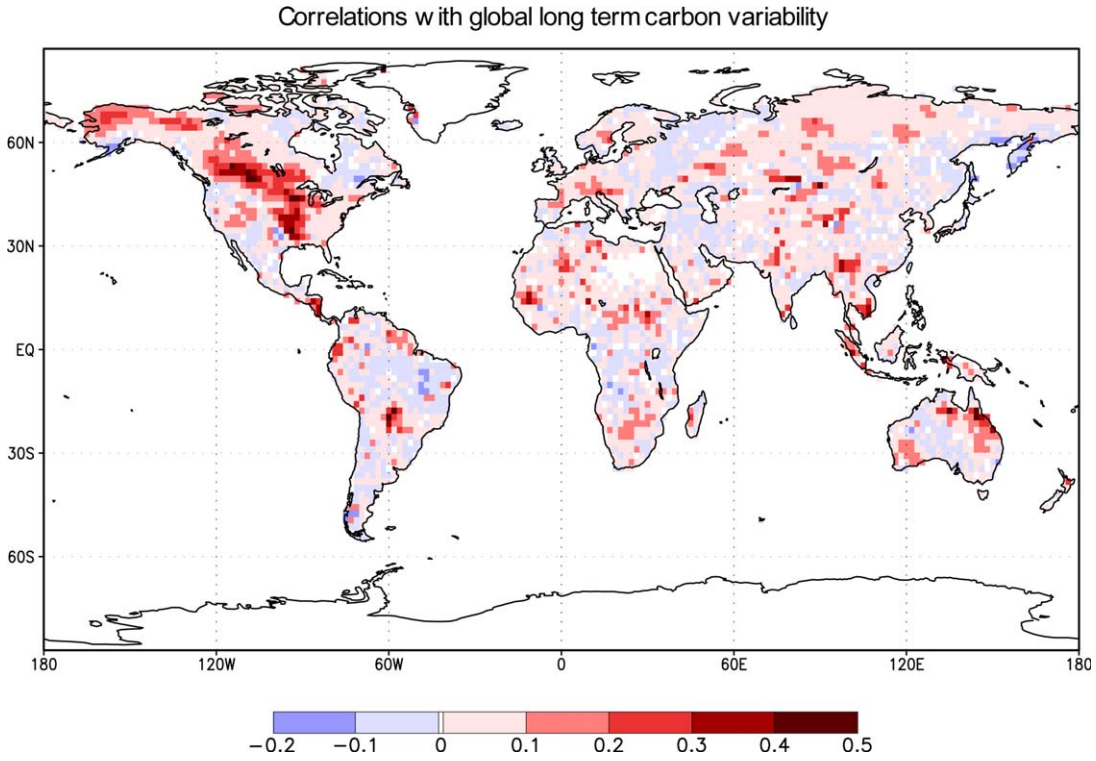

Figure 4. Pearson's R^2 of CB_fixedCO2+Veg between the terrestrial long-term carbon variation and the corresponding variations on the single grid cells. We took the 1000 year time series for each grid cell, built the 21 year running mean, and removed the long-term trends by detrending with polynomials of the order 2. The same was done for the total land average shown in Figure 2. Based on these results, we calculated Pearson's correlation

4.5. Connection Between Climate and Carbon Variability

[16] Since the variability we are interested in appears also in the simulations without vegetation dynamics (see section 4.3), and since the land C cycle does not develop its own dynamics without forcing, the C cycle variability must be climate driven. To explore the connection between climate and C storage variability in more detail, we will focus only on those grid cells that contribute clearly to the long-term C variability we are interested in. The C variations on grid cells with a correlation strength larger equal 0.1 (dark red in Figure 4) can explain large parts of the total land C variations (Figure 5). Since the land C flux between atmosphere and land is given by

$$dC/dt = \mathrm{NPP} - R_h - F - H - G,$$

where R_h denotes (heterotrophic) soil respiration, F denotes fire, H denotes harvest, and G denotes herbivory carbon fluxes; variations of total C are caused by several terms on the right-hand side of the equation. It turns out that the variations on grid cells with $R^2 \geq 0.1$ are mainly caused by NPP (about 50%) and less by soil respiration (about 25%). NPP minus soil respiration is strongly correlated with the total C flux (Pearson's $R^2 = 0.79$ and Spearman's $\rho = 0.89$ for the 21 year running means) so that F, H, and G can be excluded from the further analysis.

[17] Both NPP and soil respiration contribute to the C storage variations (on grid cells with $R^2 \geq 0.1$ as well as globally), but it is still unclear what kind of climate variability is causing these changes. Variability in soil respiration may arise from climatic causes (soil temperature and soil water) but as well as from variations in the amount of C input into soils. Therefore, soil respiration indirectly depends on NPP. To test in how far land C variations can be explained only by NPP changes we performed the CB_NPP simulation. The yearly cycle for soil temperature and water is held constant in this run, so that in this simulation soil respiration may vary only because of changes in NPP. It turns out that despite the reduced variability in the input fields for the simulation, the correlation between total land C of CB_NPP and total land C of CB_fixedCO2+Veg is high (Pearson's $R^2 = 0.68$ and Spearman's $\rho = 0.77$ for the 21 year running means). This is also true when we consider only the grid cells with $R^2 \geq 0.1$ in Figure 4 (Pearson's $R^2 = 0.76$ and Spearman's $\rho = 0.85$ for the 21 year running means). It follows that NPP and not soil temperature or soil moisture is the main pathway for the C storage variability. Further analysis reveals that the different PFTs contribute with different

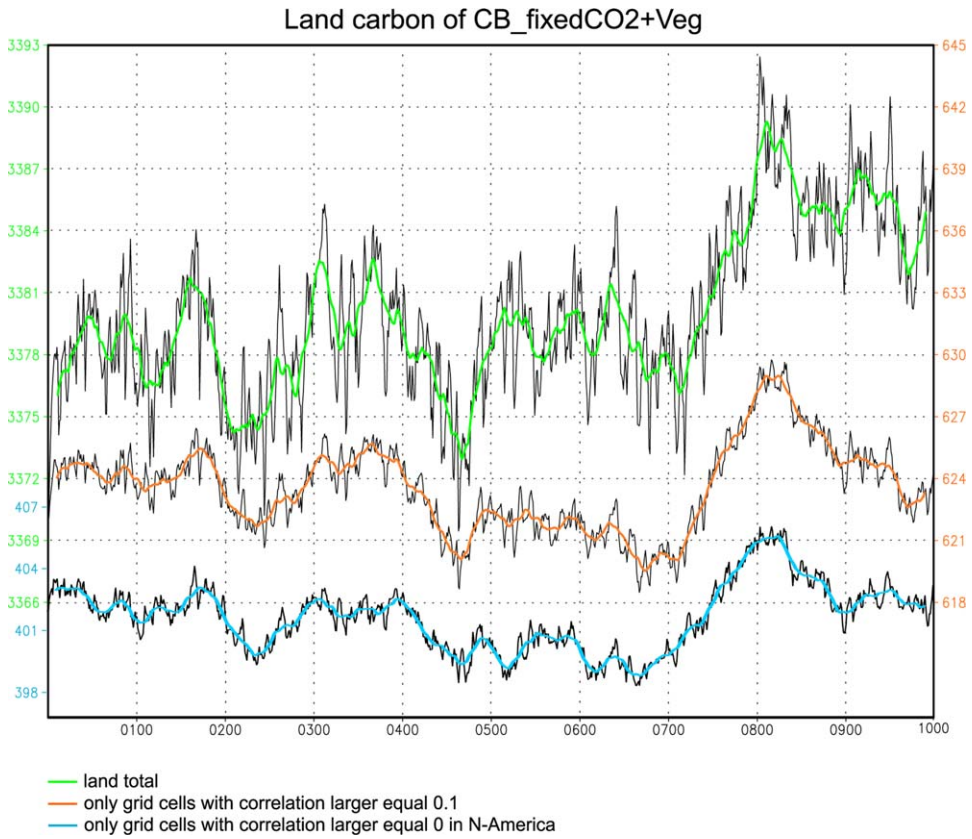

Figure 5. Sums of land carbon from CB_fixedCO2+Veg for all land points (dark green), for grid cells which are correlated to the global average with $R^2 \geq 0.1$ (orange), and for grid cells in North America which are correlated to

strengths to the NPP variability. This is also true with respect to their area coverage. Nevertheless, we could demonstrate (not shown) that the NPP variability is not confined to some specific PFTs.

[18] Continuing the search for the direct climate controls of the observed land carbon variability, we concentrate now on NPP. As already remarked earlier, NPP is itself a function of climate. In addition, NPP depends on the LAI, which is also a function of climate. Since several climate variables could cause the NPP variability, we calculated the corresponding correlation strengths (for grid cells with $R^2 \geq 0.1$) to NPP (Table 2). The same was done to obtain the correlations to the C storage changes. Table 2 shows that the climate variables (precipitation, relative soil moisture, surface temperature, incoming photosynthetic active radiation (PAR)) are not very strongly correlated with NPP or the C storage changes. In contrast to this, the absorbed photosynthetic active radiation (aPAR) is strongly correlated with NPP and the C storage. (This holds for all PFTs except the extratropical evergreen.) With including the (biotic parameter) LAI to derive aPAR from (the purely climatic) PAR, the variability in the NPP and C storage emerges. The strong correlation between LAI and NPP also indicates that LAI variations are responsible for the NPP fluctuations.

[19] In the model, the growth rate of leaves during growth seasons is computed from NPP and depends for vegetation in seasonal climates also on the length of the growth period. Dependent on the phenology type of the PFTs, the length of the growth period is a result of temperature, soil moisture, and NPP. Since the PFTs are spread over the globe and their growth period lengths depend on different climatic boundary conditions, the LAI variability is caused by different local climatic changes. To illustrate this, we calculated the correlation strength between some climate variables (surface temperature, incoming shortwave radiation, relative soil moisture) and LAI for each grid cell. Figure 6 shows that the LAI is mainly determined by soil moisture in the tropics and by surface temperature and incoming solar radiation in the extratropics.

[20] We could show that land C variability is mainly caused by NPP due to variations in the LAI and is not confined to a specific PFT or region. The connection between climate and land C variability cannot be traced back to a single climate variable.

4.6. Focus on North America

[21] The centennial land C variations are largely caused by grid cells on the North American continent (Figures 4 and 5). The connection between climate and

Table 2. Strength of Cross-Correlation Between the 21 Year Running Means of Several Climate Variables and NPP or Total Land C Flux (=dC/dt), Where the Latter Was Obtained From a CB_fixedCO2+Veg Run[a]

	NPP	Total Land C Flux
Precipitation	0.19	0.00
	0.43	−0.02
Relative soil moisture	0.01	0.20
	−0.15	−0.46
Surface temperature	0.04	0.01
	−0.19	−0.06
Incoming shortwave radiation	−0.05	0.04
	−0.22	0.20
PAR	0.04	0.04
	−0.22	0.20
aPAR	0.54	0.49
	0.73	0.69
LAI	0.66	0.28
	0.79	0.51
NPP versus total C flux		
0.46		
0.68		
Soil respiration versus total C flux		
0.00		
0.06		

[a]For all time series, only the grid cells with $R^2 \geq 0.1$ in Figure 4 are regarded. Top number represents Pearson's R^2 and is set negative to indicate anticorrelation. Bottom number represents Spearman's ρ.

C variations in North America is principally the same as described earlier, but the correlation between C storage and NPP (and respectively, LAI) gets weaker (Table 3). Instead C storage variability is more determined by soil respiration and incoming solar radiation at the surface. (Changes in incoming solar radiation are caused by cloud cover changes and are anticorrelated with soil respiration since more incoming solar radiation reduces relative soil water.) Consistent with this, the increase of the correlation strength from PAR to aPAR is much weaker. Note that this additional mechanism in North America via soil respiration does not inhibit the mechanism via NPP. When we assume a linear correlation, the regression between incoming shortwave radiation and C flux is about 0.06 PgC/(W/m^2) (for the 21 year running means of North American grid cells with $R^2 \geq 0$ in Figure 4).

5. Discussion and Conclusions

[22] In this study, we used several model runs performed with the MPI-ESM-LR to analyze C storage variations on centennial time scales. In the fully coupled run with interactively computed atmospheric CO_2 concentrations, we find centennial C variations (for the 21 year running means) of up to 6 PgC in the atmosphere,

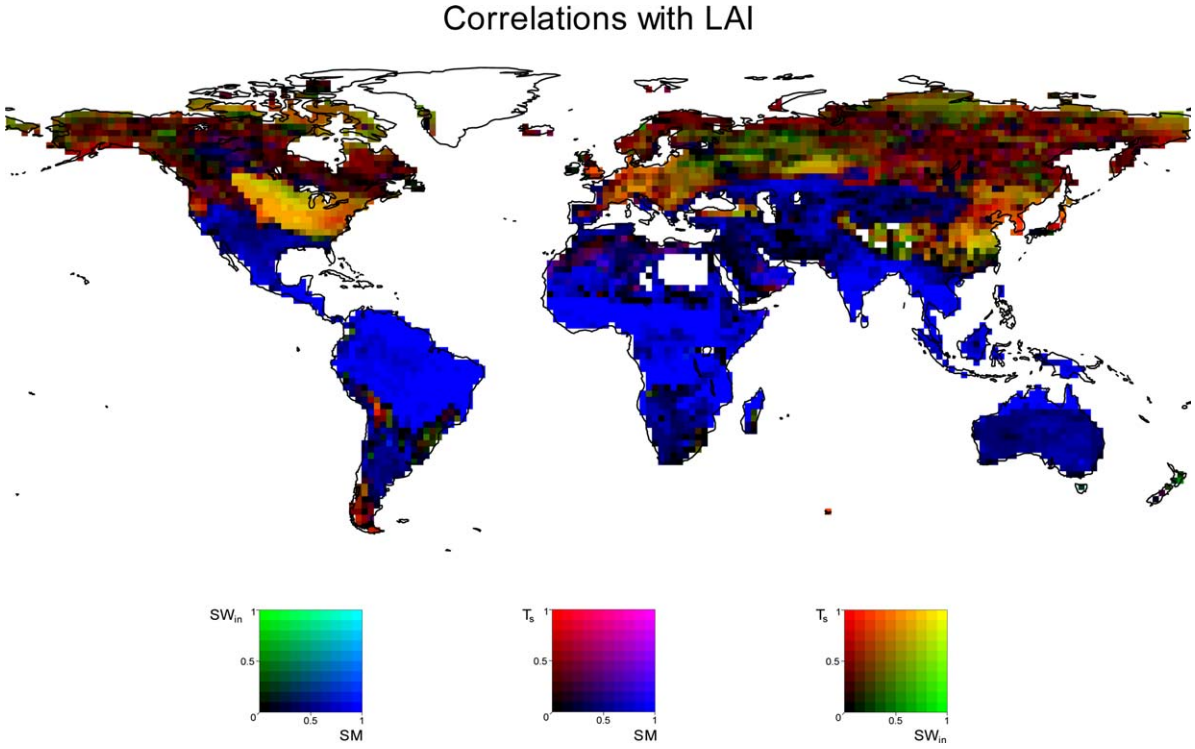

Figure 6. Map of positive correlations between climatic variables and LAI in CB_fixedCO2+Veg. Spearman's rank correlation between each climatic variable and LAI is calculated for each grid box from the 21 year running mean of the 1000 year time series. Each color in the plot is a combination of red, green, and blue. SM denotes the relative soil moisture, SWin denotes the incoming shortwave radiation at the surface, and T_s denotes the surface temperature. The intensity of red represents Spearman's ρ correlation coefficient between surface temperature and LAI for the

Table 3. As in Table 2 but for Grid Cells in North America With $R^2 \geq 0$ in Figure 4

	NPP	Total Land C Flux
Precipitation	0.00	−0.31
	0.04	−0.57
Relative soil moisture	−0.03	−0.46
	−0.20	−0.68
Surface temperature	0.12	0.20
	0.31	0.45
Incoming shortwave radiation	0.03	0.46
	0.16	0.68
PAR	0.03	0.46
	0.17	0.68
aPAR	0.32	0.49
	0.54	0.72
LAI	0.49	0.19
	0.69	0.42
NPP versus total C flux		
0.26		
0.50		
Soil respiration versus total C flux		
−0.23		
−0.45		

of up to 8 PgC for the land, and up to 4 PgC in the ocean. In our model, the centennial variations on land are much stronger than in the ocean, and the ocean acts as a buffer for the land-induced C variability. These results are in agreement with the 1000 year preindustrial simulation of *Doney et al*. [2006], which is quite comparable to our fully coupled run (see section 1). In their simulation, the C pools vary about the same amount, and C-flux variability is stronger for the land than for the ocean. They also find that the ocean tends to damp variations generated by the terrestrial biosphere.

[23] The atmospheric CO_2 variations of our model reaches up to ~3 ppm within 100 years in the 21 year running mean. This may help to understand CO_2 changes during historical times. Reconstructions of historical atmospheric CO_2 concentrations exhibit variations of about 5 ppm on time scales of centuries during the last millennium [*Reick et al*., 2010]. Approaches proposed to at least partly explain these variations are emissions from ALCCs [*Pongratz et al*., 2009; *Reick et al*., 2010] and temperature changes from volcanic or solar forcing that lead to changes in soil respiration [*Trudinger et al*., 2005; *Gerber et al*., 2003; *Mann et al*., 1999, 2008, 2009]. Our study quantifies the centennial C storage variations on land caused by internal climate variability with up to 8 PgC and in the MPI-ESM-LR run with fixed atmospheric CO_2 concentrations with up to 15 PgC. This shows that the land C variations would be nearly two times as high without the buffering effect of the ocean and the dampening of land carbon uptake by CO_2 fertilization. Therefore, with an increasing oceanic uptake saturation in the future [*Crueger et al*., 2009; *Friedlingstein et al*., 2006], natural atmospheric CO_2 variability could be even higher.

[24] In our model the centennial variability of total land C is, except for a possible contribution from the vegetation dynamics, largely passive. This variability is mainly a result of NPP variations caused by changes in the LAI. Regions all over the world contribute to these variations. *Doney et al*. [2006] find a similar mechanism: interannual-to-centennial terrestrial C-flux variability reflects primarily regional changes in NPP modulated by moisture stress. However, in our model, the climatic reason cannot be traced back to a single climatic parameter. Instead, it seems that a random superposition of climatic variations in different regions around the world result in long-term land C variations. This is also supported by the reduced significance for periods longer than 10 years in the spectral values of Figure 3.

[25] The study of *Delire et al*. [2004] with the Community Climate Model 3 coupled to the Integrated BIosphere Simulator (CCM3-IBIS) model and climatological sea surface temperatures shows that vegetation dynamics may increase long-term variability in the climate system on time scales between a decade and a century. Slow changes in the vegetation cover of the dynamic vegetation are responsible for this long-term variability (due to the positive feedbacks between precipitation and LAI). In their study "vegetation cover" means expressed more exactly "peak LAI reached during the year." Therefore, changes in the "vegetation cover" are not necessarily changes in the plant cover fractions but could also be changes in peak LAI on unmodified cover fractions. For the latter case, their results agree with ours, which indicate that long-term terrestrial LAI variations occur in similar strength with or without the spreading and withdrawal of vegetation.

[26] We find a pronounced land C variability in North America, which is strongly correlated with incoming shortwave radiation at the surface. The regression between incoming shortwave radiation and C flux for the 21 year running means is about 0.06 PgC/(W/m^2). *Liepert* [2002] shows that the 10 year average of incoming solar radiation in the United States decreased by 19 W/m^2 from the 1960s to the 1980s with the strongest decline in the second decade (13 W/m^2). If we assume the above-named regression of 0.06 PgC/(W/m^2), the dimming effect of 19 W/m^2 would reduce the C storage by 1.14 PgC. However, a dimming effect by anthropogenic aerosols increases the fraction of incoming diffuse radiation, which would probably increase NPP [*Mercado et al*., 2009] and is not considered in this calculation. For comparison, carbon stock in living biomass in the United States increased between 2000 and 2010 by only 1.31×10^{-3} PgC and, if the reduced carbon stock in Canada is included, by only 9×10^{-4} PgC [*Food and Agriculture Organization*, 2011]. *Nabuurs et al*. [2007] estimate the (economic) potential of C storage by afforestation and forest management with 0.11–0.22 PgC/yr for North America (values annualized till 2040). Thus, the potential C storage increase by afforestation and forest management would take more than 10 years to sum up to the same order of magnitude as the model indicated C storage loss in consequence of 20 years of dimming. As a conclusion, global dimming has at least the potential to affect land C storage.

[27] **Acknowledgments.** We gratefully acknowledge the comments of our two anonymous reviewers.

References

Ahn, J., E. J. Brook, L. Mitchell, J. Rosen, J. R. McConnell, K. Taylor, D. Etheridge, and M. Rubino (2012), Atmospheric CO2 over the last 1000 years: A high-resolution record from the West Antarctic Ice Sheet (WAIS) Divide ice core, *Global Biogeochem. Cycles*, *26*, GB2027, doi:10.1029/2011GB004247.

Bacastow, R. B. (1976), Modulation of atmospheric carbon dioxide by the southern oscillation, *Nature*, *261*(5556), 116–118, doi:10.1038/261116a0.

Bacastow, R. B., J. A. Adams, C. D. Keeling, D. J. Moss, T. P. Whorf, and C. S. Wong (1980), Atmospheric carbon dioxide, the southern oscillation, and the weak 1975 El Nino, *Science*, *210*(4465), 66–68, doi:10.1126/science.210.4465.66.

Bosquet, P., P. Peylin, P. Ciais, C. Le Quere, P. Friedlingstein, and P. P. Tans (2000), Regional changes in carbon dioxide fluxes of land and oceans since 1980, *Science*, *290*, 1342–1346, doi:10.1126/science.290.5495.1342.

Bretagnon, P., and G. Francou (1988), Planetary theories in rectangular and spherical variables—VSOP 87 solutions, *Astron. Astrophys.*, *202*, 309–315.

Brovkin, V., A. Ganopolski, D. Archer, and S. Rahmstorf (2007), Lowering of glacial atmospheric CO2 in response to changes in oceanic circulation and marine biogeochemistry, *Paleoceanography*, *22*(4), 1–14, doi:10.1029/2006PA001380.

Brovkin, V., T. Raddatz, C. H. Reick, M. Claussen, and V. Gayler (2009), Global biogeophysical interactions between forest and climate, *Geophys. Res. Lett.*, *36*, L07405, doi:10.1029/2009GL037543.

Brovkin, V., S. J. Lorenz, J. Jungclaus, T. Raddatz, C. Timmreck, C. H. Reick, J. Segschneider, and K. Six (2010), Sensitivity of a coupled climate-carbon cycle model to large volcanic eruptions during the last millennium, *Tellus B*, *62*(5), 674–681, doi:10.1111/j.1600-0889.2010.00471.x.

Caillon, N., J. P. Severinghaus, J. Jouzel, J.-M. Barnola, J. Kang, and V. Y. Lipenkov (2003), Timing of atmospheric CO2 and Antarctic temperature changes across termination III, *Science*, *299*(5613), 1728–1731, doi:10.1126/science.1078758.

Collatz, G. J., M. Ribas-Carbo, and J. A. Berry (1992), Coupled photosynthesis-stomatal conductance model for leaves of C4 plants, *Aust. J. Plant Physiol.*, *19*, 519–538, doi:10.1071/PP9920519.

Crueger, T., E. Roeckner, R. Schnur, T. Raddatz, and P. Wetzel (2009), Slow-down of oceanic CO2 uptake in response to global warming, in *Marine Phytoplankton*, edited by W. T. Kersey and S. P. Munger, Nova Science Publishers, Hauppage, USA. pp. 89–121.

Delire, C., J. Foley, and S. Thompson (2004), Long-term variability in a coupled atmosphere–biosphere model, *J. Clim.*, *17*, 3947–3959, doi:10.1175/1520-0442(2004)017<3947:LVIACA>2.0.CO;2.

Doney, S. C., and D. S. Schimel (2007), Carbon and climate system coupling on timescales from the Precambrian to the Anthropocene, *Annu. Rev. Environ. Resour.*, *32*(1), 31–66, doi:10.1146/annurev.energy.32.041706.124700.

Doney, S. C., K. Lindsay, I. Fung, and J. John (2006), Natural variability in a stable, 1000-yr global coupled climate-carbon cycle simulation, *J. Clim.*, *19*, 3033–3054, doi:10.1175/JCLI3783.1.

Enting, I., T. M. L. Wigley, and M. Heimann (1994), Future emissions and concentrations of carbon dioxide: Key ocea00tmosphere/land analyses, *CSIRO Div. Atmos. Res. Tech. Pap. 31*, 133 pp.

Etheridge, D. M., L. P. Steele, R. L. Langenfelds, R. J. Francey, J.-M. Barnola, and V. I. Morgan (1996), Natural and anthropogenic changes in atmospheric CO2 over the last 1000 years from air in Antarctic ice and firn, *J. Geophys. Res.*, *101*(D2), 4115–4128, doi:10.1029/95JD03410.

Food and Agriculture Organization (2011), State of the World's Forests, 164 pp., Food and Agric. Organ. of the U. N., Rome. [Available at http://www.fao.org/docrep/013/i2000e/i2000e00.htm.].

Farquhar, G. D., S. von Caemmerer, and J. A. Berry (1980), A biogeochemical model of photosynthesis in leaves of C3 species, *Planta*, *149*(1), 78–90, doi:10.1007/BF00386231.

Forster, P., et al. (2007), Changes in atmospheric constituents and in radiative forcing, in *Contribution of Working Group I to the Fourth Assessment Report of the Intergovernmental Panel on Climate Change*, edited by S. D. Solomon et al., pp. 129–234, Cambridge Univ. Press, Cambridge, U. K.

Friedlingstein, P., et al. (2006), Climate-Carbon cycle feedback analysis: Results from the C4MIP model intercomparison, *J. Clim.*, *19*(14), 3337–3354, doi:10.1175/JCLI3800.1.

Gerber, S., F. Joos, P. Brügger, T. F. Stocker, M. E. Mann, S. Sitch, and M. Scholze (2003), Constraining temperature variations over the last millennium by comparing simulated and observed atmospheric CO2, *Clim. Dyn.*, *20*, 281–299, doi:10.1007/s00382-002-0270-8.

Giorgetta, M., et al. (2012), CMIP5 simulations of the Max Planck Institute for Meteorology (MPI-M) based on the MPI-ESM-LR model: The piControl experiment, served by ESGF, World Data Center for Climate, doi:10.1594/WDCC/CMIP5.MXELpc. http://cera-www.dkrz.de/WDCC/CMIP5/Compact.jsp?acronym=MXELpc.

Hansen, J., and M. Sato (2004), Greenhouse gas growth rates, *Proc. Natl. Acad. Sci. U. S. A.*, *101*(46), 16,109–16,114, doi:10.1073/pnas.0406982101.

Joos, F., R. Meyer, M. Bruno, and M. Leuenberger (1999), The variability in the carbon sinks as reconstructed for the last 1000 years, *Geophys. Res. Lett.*, *26*(10), 1437–1440, doi:10.1029/1999GL900250.

Jungclaus, J. H., et al. (2010), Climate and carbon-cycle variability over the last millennium, *Clim. Past*, *6*(5), 723–737, doi:10.5194/cp-6–723-2010.

Keeling, C. D., and T. P. Whorf (1995), Decadal oscillations in global temperature and atmospheric carbon dioxide, in *Natural Climate Variability On Decade-to-Century Time Scales*, edited by Climate Research Committee, Board on Atmospheric Sciences and Climate, Commission on Geosciences, Environment, and Resources, National Research Council, pp. 97–106, Natl. Acad. Press, Washington, D. C.

Keeling, R. F., P. Raymond, M. L. Bender, and P. P. Tans (1993), What atmospheric oxygen measurements can tell us about the global carbon cycle, *Global Biogeochem. Cycles*, *7*(1), 37–67, doi:10.1029/92GB02733.

Knorr, W. (2000), Annual and interannual CO2 exchanges of the terrestrial biosphere: Process-based simulations and uncertainties, *Global Ecol. Biogeogr.*, *9*, 225–252, doi:10.1046/j.1365–2699.2000.00159.x.

Liepert, B. G. (2002), Observed reductions of surface solar radiation at sites in the United States and worldwide from 1961 to 1990, *Geophys. Res. Lett.*, *29*(10), 1–4, doi:10.1029/2002GL014910.

Lloyd, J., and J. A. Taylor (1994), On the temperature dependence of soil respiration, *Funct. Ecol.*, *8*, 315–323.

Lüthi, D. et al. (2008), High-resolution carbon dioxide concentration record 650,000–800,000 years before present, *Nature*, *453*(7193), 379–382, doi:10.1038/nature06949.

MacFarling Meure, M. C., D. M. Etheridge, M. C. Trudinger, P. Steele, R. Langenfelds, T. van Ommen, A. Smith, and J. Elkins (2006), Law Dome CO2, CH4 and N2O ice core records extended to 2000 years BP, *Geophys. Res. Lett.*, *33*, L14810, doi:10.1029/2006GL026152.

Mann, M. E., R. S. Bradley, and M. K. Hughes (1999), Northern hemisphere temperatures during the past millennium: Inferences, uncertainties, and limitations, *Geophys. Res. Lett.*, *26*(6), 759–762, doi:10.1029/1999GL900070.

Mann, M. E., Z. Zhang, M. K. Hughes, R. S. Bradley, S. K. Miller, S. Rutherford, and F. Ni (2008), Proxy-based reconstructions of hemispheric and global surface temperature variations over the past two millennia, *Proc. Natl. Acad. Sci. U. S. A.*, *105*(36), 13,252–13,257, doi:10.1073/pnas.0805721105.

Mann, M. E., Z. Zhang, S. Rutherford, R. S. Bradley, M. K. Hughes, D. Shindell, C. Ammann, G. Faluvegi, and F. Ni (2009), Medieval climate anomaly, *Science*, *326*, 1256–1260.

Mercado, L. M., N. Bellouin, S. Sitch, O. Boucher, C. Huntingford, M. Wild, and P. M. Cox (2009), Impact of changes in diffuse radiation on the global land carbon sink, *Nature*, *458*, 1014–1018, doi:10.1038/nature07949.

Nabuurs, G. J., et al. (2007), Forestry, in *Climate Change 2007: Mitigation. Contribution of Working Group III to the Fourth Assessment Report of the Intergovernmental Panel on Climate Change,* edited by B. Metz et al., Cambridge Univ. Press, Cambridge, U. K.

Otto, J., T. Raddatz, and M. Claussen (2011), Strength of forest albedo feedback in mid-Holocene climate simulations, *Clim. Past*, *7*, 1027–1039, doi:10.5194/cp-7–1027-2011.

Pearson, P. N., and M. R. Palmer (2000), Atmospheric carbon dioxide concentrations over the past 60 million years, *Nature*, *406*(6797), 695–699, doi:10.1038/35021000.

Petit, R. J. et al. (1999), Climate and atmospheric history of the past 420,000 years from the Vostok ice core, Antarctica, *Nature*, *399*, 429–436, doi:10.1038/20859.

Pinter, N., S. Fiedel, and J. E. Keeley (2011), Fire and vegetation shifts in the Americas at the vanguard of Paleoindian migration, *Quat. Sci. Rev.*, *30*(3–4), 269–272, doi:10.1016/j.quascirev.2010.12.010.

Pongratz, J., C. H. Reick, T. Raddatz, and M. Claussen (2009), Effects of anthropogenic land cover change on the carbon cycle of the last millennium, *Global Biogeochem. Cycles*, *23*, GB4001, doi:10.1029/2009GB003488.

Pongratz, J., C. H. Reick, T. Raddatz, and M. Claussen (2010), Biogeophysical versus biogeochemical climate response to historical anthropogenic land cover change, *Geophys. Res. Lett.*, *37*, L08702, doi:10.1029/2010GL043010.

Prentice, I. C., G. D. Farquhar, M. J. R. Fasham, M. L. Goulden, M. Heimann, V. J. Jaramillo, H. S. Kheshgi, C. Le Quere, R. J. Scholes, and D. W. R. Wallace (2001), The carbon cycle and atmospheric carbon dioxide, in *Climate Change 2001: The Physical Science Basis. Contribution of Working Group I to the Third Assessment Report of the Intergovernmental Panel on Climate Change*, edited by J. T. Houghton et al., Cambridge Univ. Press, Cambridge, U. K.

Press, W. H., S. A. Teukolsky, W. T. Vetterling, and B. P. Flannery (1992), *Numerical Recipes in C: The Art of Scientific Computing*, 2nd ed., Cambridge Univ. Press, Cambridge, UK.

Raddatz, T. J., C. J. Reick, W. Knorr, J. Kattge, E. Roeckner, R. Schnur, K.-G. Schnitzler, P. Wetzel, and J. Jungclaus (2007), Will the tropical land biosphere dominate the climate-carbon cycle feedback during the twenty-first century?, *Clim. Dyn.*, *29*, 565–574, doi:10.1007/s00382-007-0247-8.

Rayner, P. J., and Law, R. M. (1999), The relationship between tropical CO2 fluxes and the El Nino-Southern Oscillation, *Geophys. Res. Lett.*, *26*(4), 493–496, doi:10.1029/1999GL900008.

Reick, C. H., T. Raddatz, J. Pongratz, and M. Claussen (2010), Contribution of anthropogenic land cover change emissions to pre-industrial atmospheric CO2, *Tellus B*, *62*(5), 329–336, doi:10.1111/j.1600-0889.2010.00479.x.

Robock, A. (2003), Introduction: Mount Pinatubo as a test of climate feedback mechanisms, in *Volcanism and the Earth's Atmosphere, Geophys. Monogr.*, vol. *139*, edited by A. Robock and C. Oppenheimer, pp. 1–8, AGU, Washington, D. C,.

Roeckner, E., et al. (2003), *The atmospheric general circulation model ECHAM 5. PART I: Model description, MPI Rep. 349*, Max Planck Inst. for Meteorol., Hamburg, Germany. [Available at http://www.mpimet.mpg.de/fileadmin/publikationen/Reports/max_scirep_349.pdf.].

Ruddiman, W. F., J. E. Kutzbach, and S. J. Vavrus (2011), Can natural or anthropogenic explanations of late-Holocene CO2 and CH4 increases be falsified?, *Holocene*, *21*(5), 865–879, doi:10.1177/0959683610387172.

Schwalm, C. R., C. A. Williams, K. Schaefer, I. Baker, and G. J. Collatz (2011), Does terrestrial drought explain global atmospheric CO2 flux anomalies induced by ENSO?, *Biogeosciences*, *8*, 2493–2506, doi:10.5194/bg-8–2493-2011.

Siegenthaler, U., et al. (2005a), Stable carbon cycle-climate relationship during the Late Pleistocene, *Science*, *310*(5752), 1313–1317, doi:10.1126/science.1120130, doi:10.1111/j.1600-0889.2005.00131.x.

Siegenthaler, U., E. Monnin, K. Kawamura, R. Spahni, J. Schwander, B. Stauffer, T. F. Stocker, J.-M. Barnola, and H. Fischer (2005b), Supporting evidence from the EPICA Dronning Maud Land ice core for atmospheric CO2 changes during the past millennium, *Tellus B*, *57*(1), 51–57.

Sigman, D. M., and E. A. Boyle (2000), Glacial/interglacial variations in atmospheric carbon dioxide, *Nature*, *407*(6806), 859–869, doi:10.1038/35038000.

Stocker, B. D., K. Strassmann, and F. Joos (2011), Sensitivity of Holocene atmospheric CO2 and the modern carbon budget to early human land use: Analyses with a process-based model, *Biogeosciences*, *8*(1), 69–88, doi:10.5194/bg-8–69-2011.

Taylor, K. E., R. J. Stouffer, and G. A. Meehl (2011a), *A Summary of the CMIP5 Experiment Design*. [Available at http://cmip-pcmdi.llnl.gov/cmip5/docs/Taylor_CMIP5_design.pdf.].

Taylor, K. E., V. Balaji, S. Hankin, M. Juckes, B. Lawrence, and S. Pascoe (2011b), CMIP5 data reference syntax (DRS) and controlled vocabularies. [Available at http://cmip-pcmdi.llnl.gov/cmip5/docs/cmip5_data_reference_syntax.pdf.].

Taylor, K. E., R. J. Stouffer, and G. A. Meehl (2012), An overview of CMIP5 and the experiment design, *Bull. Am. Meteorol. Soc.*, *93*, 485–498, doi:10.1175/BAMS-D-11–00094.1.

Trudinger, C. M., I. G. Enting, and R. J. Francey (1999), Long-term variability in the global carbon cycle inferred from a high-precision CO2 and δ13C ice-core record. *Tellus B*, *51*, 233–248, doi:10.1034/j.1600-0889.1999.t01-1-00009.x.

Trudinger, C. M., I. G. Enting, P. J. Rayner, and R. J. Francey (2002), Kalman filter analysis of ice core data: 2. Double deconvolution of CO2 and δ13C measurements, *J. Geophys. Res.*, *107*(D20), 4423, doi:10.1029/2001JD001112.

Trudinger, M. C., I. Enting, D. M. Etheridge, R. Francey, and P. Rayner (2005), The carbon cycle over the past 1000 years inferred from the inversion of ice core data, in *Ecological Studies*, edited by M. D. Ehleringer, J. R. Cerling, and T. E. Dearing, pp. 329–349, Springer, New York, doi:10.1007/0–387-27048-5_15.

Williams, M. (2003), *Deforesting the Earth: From Prehistory to Global Crisis*, Univ. of Chicago Press, Chicago, Ill.

Wolf, A., P. Ciais, V. Bellassen, N. Delbart, C. B. Field, and J. A. Berry (2011), Forest biomass allometry in global land surface models, *Global Biogeochem. Cycles*, *25*, GB3015, doi:10.1029/2010GB003917.

Zachos, J. C., H. Pagani, L. Sloan, E. Thomas, and K. Billups (2001), Trends, rhythms, and aberrations in global climate 65 Ma to present, *Science*, *292*(5517), 686–693, doi:10.1126/science.1059412.

Zachos, J. C., G. R. Dickens, and R. E. Zeebe (2008), An early Cenozoic perspective on greenhouse warming and carbon-cycle dynamics, *Nature*, *451*(7176), 279–283, doi:10.1038/nature06588.

Corresponding author: R. Schneck, Max Planck Institute for Meteorology, Bundesstraße 53, D-20146 Hamburg, Germany. (rainer.schneck@zmaw.de)